K. E. Goodson[1]

M. I. Flik

Department of Mechanical Engineering.

L. T. Su

D. A. Antoniadis

Department of Electrical Engineering and Computer Science.

Massachusetts Institute of Technology, Cambridge, MA 02139

Prediction and Measurement of the Thermal Conductivity of Amorphous Dielectric Layers

Thermal conduction in amorphous dielectric layers affects the performance and reliability of electronic circuits. This work analyzes the influence of boundary scattering on the effective thermal conductivity for conduction normal to amorphous silicon dioxide layers, $k_{n,eff}$. At 10 K, the predictions agree well with previously reported data for deposited layers, which show a strong reduction of $k_{n,eff}$ compared to the bulk conductivity, k_{bulk}. A steady-state technique measures $k_{n,eff}$ near room temperature of silicon dioxide layers fabricated using oxygen-ion implantation (SIMOX). The predictions and the SIMOX data, which agree closely with k_{bulk}, show that boundary scattering is not important at room temperature. Lower than bulk conductivities of silicon dioxide layers measured elsewhere near room temperature must be caused by interfacial layers or differences in microstructure or stoichiometry.

1 Introduction

The performance of transistors and the reliability of interconnects are affected by temperature fields in electronic circuits. Layers of amorphous dielectric materials electrically insulate circuit components and protect them from corrosion. These layers have very low thermal conductivities, near 1 $Wm^{-1}K^{-1}$ at room temperature. Conduction normal to the layers can be an important obstacle to the cooling of devices and interconnects. Energy dissipated in aluminum interconnects in conventional integrated circuits, for example, must travel through an amorphous silicon dioxide layer between 0.5 and 1 μm thick to reach the substrate heat sink. In silicon-on-insulator (SOI) circuits, devices are separated from the substrate by a silicon dioxide layer from 0.3 to 1.0 μm thick (Goodson and Flik, 1992; Goodson et al., 1993b). To predict the mean time to failure of an interconnect or the drain current of a SOI field-effect transistor, both of which depend on temperature, a circuit designer needs to know the thermal resistance for conduction normal to amorphous dielectric layers. Most experimental techniques cannot separate the internal thermal resistance for conduction normal to a layer from the thermal resistances of its boundaries. They measure the effective thermal conductivity normal to a layer, $k_{n,\text{eff}}$, which is defined as the layer thickness divided by the total thermal resistance of the layer *and its boundaries*.

Data for the thermal conductivity of bulk amorphous dielectrics, k_{bulk}, vary little among different samples of the same material (Berman, 1976). In contrast, data for $k_{n,\text{eff}}$ of amorphous dielectric layers vary substantially and can be an order of magnitude less than k_{bulk}. Figure 1 compares the data of Lambropoulos et al. (1989), Brotzen et al. (1992), and Schafft et al. (1989) for $k_{n,\text{eff}}$ of silicon dioxide layers fabricated using several techniques. The layers of Schafft et al. (1989) contained 4 mass percent of phosphorus, whose influence on the conductivity has not been assessed. Although different experimental techniques were used, often yielding unknown or very large uncertainties, the data indicate that the effective conductivity decreases with decreasing layer thickness and depends on the fabrication technique. This is consistent with earlier data for amorphous dielectric layers (Guenther and McIver, 1988).

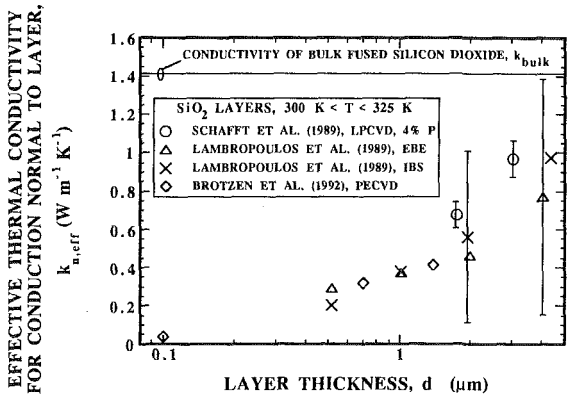

Fig. 1 Previous data for the effective thermal conductivity for conduction normal to silicon dioxide layers, $k_{n,\text{eff}}$. LPCVD = low-pressure chemical-vapor deposition. EBE = electron-beam evaporation. IBS = ion-beam sputtering. PECVD = plasma-enhanced chemical-vapor deposition. The layers of Schafft et al. (1989) contained 4 mass percent of phosphorus atoms. The bulk conductivity k_{bulk} was measured by Sugawara (1969).

The difference between $k_{n,\text{eff}}$ and k_{bulk} has been attributed to three phenomena: (*a*) Schafft et al. (1989) indicated that the boundary scattering of phonons is responsible. (*b*) A microstructure or stoichiometry in the layers different than in the bulk could make $k_{n,\text{eff}}$ smaller than k_{bulk}. The conductivity $k_{n,\text{eff}}$ would be thickness dependent if the microstructure or stoichiometry changed near the layer boundaries. (*c*) A thermal boundary resistance would cause $k_{n,\text{eff}}$ to decrease with decreasing layer thickness. This would be indistinguishable from the highly resistive interfacial layers proposed by Brotzen et al. (1992). The present work makes progress toward resolving this puzzle by predicting the effective conductivity normal to amorphous silicon dioxide layers considering (*a*) phonon-boundary scattering, and by measuring the effective conductivity of layers with varying thicknesses with a known accuracy. The data and predictions yield conclusions about the importance of (*b*) and (*c*).

Thermal conduction in bulk amorphous solids was reviewed by Zaitlin and Anderson (1975), Berman (1976), and Freeman and Anderson (1986b). Figure 2 shows the difference between the periodic structure of a crystal and the random network of atoms in an amorphous material. Phonons of wavelength small compared to the lattice constant of the material in crystalline

[1]Present address: Daimler Benz AG, Forschung und Technik (F1W/FF), 89013 Ulm, Federal Republic of Germany.

Contributed by the Heat Transfer Division for publication in the JOURNAL OF HEAT TRANSFER. Manuscript received by the Heat Transfer Division January 1993; revision received July 1993. Keywords: Conduction, Electronic Equipment, Measurement Techniques. Associate Technical Editor: R. Viskanta.

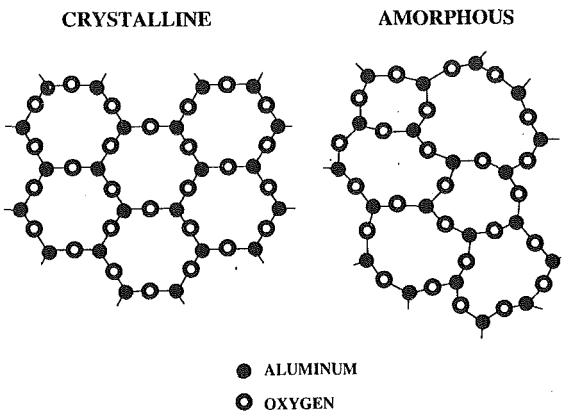

Fig. 2 Spatial configurations of atoms in two-dimensional analogs of crystalline and amorphous Al_2O_3 (after Zachariasen, 1932)

form are scattered strongly by the disorder and have mean free paths of a few angstroms (Kittel, 1949, 1986). Phonons of wavelength large compared to this lengthscale have mean free paths that increase rapidly with the wavelength. This is analogous to the Rayleigh scattering of radiation on particles small compared to the radiation wavelength, where the photon mean free path is proportional to the fourth power of the wavelength (Bohren and Huffman, 1983). The scattering of the long-wavelength phonons on the boundaries of a layer can strongly reduce $k_{n,\text{eff}}$ at cryogenic temperatures, where these phonons carry much of the thermal energy.

Many studies of phonon-boundary scattering in amorphous materials were for low temperatures. The analysis and data of Matsumoto et al. (1977) showed that the boundary scattering of long-wavelength phonons strongly reduces the effective thermal conductivity normal to epoxy layers with thicknesses between 1 and 10 μm below 10 K. But Zaitlin et al. (1975) observed no effect of boundary scattering on the thermal conductivity along 2.9 to 71 μm thick mylar and glass layers below 10 K. This was attributed to the specular reflection of phonons at the layer boundaries, which reduces conduction normal to a layer but does not affect conduction along the layer. Zhu and Anderson (1990) measured the thermal conductivities of epoxies filled with epoxy particles below 9 K, and concluded that phonons had an increased rate of scattering near the particle boundaries, analogous to hypothesis (*c*) given here. Love and Anderson (1990) developed a function for the dependence of the phonon mean free path on the phonon frequency. They predicted that phonons with mean free paths longer than about 10 Å contribute significantly to thermal conduction only at temperatures below 50 K. While they did not consider conduction in layers, their calculations indicate that phonon-boundary scattering is unimportant in silicon dioxide layers above 50 K. This cannot be confirmed by the room-temperature data shown in Fig. 1, which all show a strong reduction of $k_{n,\text{eff}}$ with respect to k_{bulk}.

The present work predicts the influence of boundary scattering on the effective conductivity normal to silicon-dioxide layers above 10 K using a frequency dependence of the phonon mean free path similar to that of Love and Anderson (1990). The effective conductivity considering boundary scattering is calculated using the approximate relations of Matsumoto et al. (1977) and Chen and Tien (1992). The technique of Swartz and Pohl (1987) is adapted to measure $k_{n,\text{eff}}$ near room temperature in silicon dioxide layers fabricated using oxygen-ion implantation (SIMOX), and a general expression for the uncertainty of the technique is developed.

2 Effective Conductivity Considering Boundary Scattering

The kinetic formula for the conductivity of dielectrics is (Ziman, 1960),

$$k = \frac{1}{3} C_s v_s \Lambda_s \tag{1}$$

where C_s is the phonon specific heat per unit volume and v_s is the speed of sound. Equation (1) defines the phonon mean free path Λ_s accounting for phonons *of all frequencies*. The *frequency-dependent* phonon mean free path, Λ_ω, is the mean distance phonons of a given frequency, or energy, travel between collisions. The use of the phonon mean free path Λ_s neglects the energy dependence of the carrier free paths. This approximation has been used with reasonable success to analyze electron-boundary scattering (Tien et al., 1969; Flik and Tien, 1990; Kumar and Vradis, 1991), since electrons contributing to net transport all possess nearly the same energy. But in dielectrics, where phonons of energies varying by several orders of magnitude contribute to conduction, Λ_s must be used with care. This was demonstrated by Savvides and Goldsmid (1972), who observed boundary-scattering effects on the phonon conductivity in silicon crystals of dimensions orders of magnitude larger than Λ_s. The crystals had been irradiated

Nomenclature

a = dimension of scattering site, m
B = boundary-scattering parameter, Eqs. (4) and (5)
C_s = phonon specific heat at constant volume per unit volume, $\text{Jm}^{-3}\text{K}^{-1}$
$C_s(x, T)$ = Debye specific heat function, defined by Eq. (3), $\text{Jm}^{-3}\text{K}^{-1}$
d = layer thickness, m
d_{sub} = substrate thickness, m
E_0 = fitting parameter for Λ_{SR}, J
h_P = Planck's constant divided by $2\pi = 1.05 \times 10^{-34}$Js
I = current, A
i = integer in summations, Eqs. (12) and (13)
k_B = Boltzmann constant $= 1.38 \times 10^{-23}\text{JK}^{-1}$
k_{bulk} = thermal conductivity measured in bulk samples, $\text{Wm}^{-1}\text{K}^{-1}$
$k_{n,\text{eff}}$ = effective thermal conductivity for conduction normal to layer, $\text{Wm}^{-1}\text{K}^{-1}$
k_{sub} = substrate thermal conductivity, $\text{Wm}^{-1}\text{K}^{-1}$
L = length, m
N_a = atomic number density, m^{-3}
N_D = number density of scattering sites, m^{-3}
Q = heat flow, W
q = argument of relative uncertainty function $= U(q)$
R_T = thermal resistance, m^2KW^{-1}
S_D = fitting parameter for Λ_D, $\text{m rad}^4\text{s}^{-4}$
S_{SR} = fitting parameter for Λ_{SR}
T = temperature, K
ΔT = temperature difference, K
T^* = $k_B T/E_0$ = dimensionless temperature
T_B = average substrate temperature below bridge A, K
T_0 = substrate or chuck temperature, K
$U(q)$ = relative uncertainty in parameter q
V = voltage difference along bridge, V
v_s = average speed of sound, ms^{-1}
W = half width of substrate, m
w = width, m
x = dimension along substrate, m

with neutrons, introducing point defects that cause the Rayleigh scattering of phonons.

Equation (1) can be written as an integral over all phonon angular frequencies ω using the Debye model for phonons (Berman, 1976)

$$k=\frac{1}{3}v_s\int_0^{\theta/T} C_s[x_\omega, T]\Lambda_\omega[x_\omega, T]dx_\omega \tag{2}$$

where the Debye specific heat function is

$$C_s[x_\omega, T]=9N_a k_B\left(\frac{T}{\theta}\right)^3\frac{(x_\omega)^4\exp(x_\omega)}{[\exp(x_\omega)-1]^2} \tag{3}$$

The dimensionless phonon frequency is $\chi_\omega=h_p\omega/k_\beta T$. The Debye model constants for amorphous silicon dioxide are $\theta=492$ K, $v_s=4100$ ms^{-1}, and $N_a=6.62\times10^{28}$ m^{-3} (Stephens, 1973). The Debye angular frequency is $\omega_D=k_B\theta/h_P=6.441\times10^{13}$ rads^{-1}.

If the material is bulk, i.e., has no boundaries, then Λ_ω is the bulk mean free path, $\Lambda_{\omega,\text{bulk}}$. Callaway (1959) and Holland (1963) accounted for boundary scattering using a frequency-independent mean free bath for boundary scattering, $\Lambda_{s,b}=Bd$, where B is a dimensionless constant not too far from unity and d is the smallest specimen dimension, e.g., the layer thickness. Matthiessen's rule (Ziman, 1960) yields

$$\frac{1}{\Lambda_\omega}=\frac{1}{\Lambda_{\omega,\text{bulk}}}+\frac{1}{\Lambda_{s,b}}=\frac{1}{\Lambda_{\omega,\text{bulk}}}+\frac{1}{Bd} \tag{4}$$

Matsumoto et al. (1977) used Eqs. (2)–(4) to calculate $k_{n,\text{eff}}$ for epoxy layers below 10 K. They assumed a frequency and temperature dependence for $\Lambda_{\omega,\text{bulk}}$ and fitted bulk epoxy thermal conductivity data using $d=\infty$, i.e., $\Lambda_\omega=\Lambda_{\omega,\text{bulk}}$. The predicted temperature dependence of $k_{n,\text{eff}}$ agreed with the data for layers when B was used as an adjustable parameter.

The nature of phonon reflection and transmission at the boundaries depends on the ratio of the phonon wavelength to the standard deviation of the boundary profile (Ziman, 1960). When this ratio is near or smaller than unity, the phonons are reflected and transmitted diffusely. At room temperature, phonons with wavelengths from a few angstroms to a few tens of nanometers contribute to energy transport. The shortest wavelength phonons, which carry most of the energy, are diffusely reflected by any practical interface. The longest wavelength phonons may not scatter diffusely on the boundaries of many interfaces. Swartz and Pohl (1989) derived the approximate diffuse mismatch model for the diffuse transmission and reflection of phonons at an interface, and showed that the boundary resistance predicted by this model agrees well with data for metal–dielectric interfaces and differs little from that predicted by the theory of Little (1959) for an ideal smooth interface. The diffuse mismatch model is used here for the transmission coefficients of phonons of all wavelengths. The error due to the non-diffuse transmission and specular reflection of long wavelength phonons at the boundaries is expected to be small, but has not been quantified.

The diffuse mismatch model assumes complete contact between the layer and the bounding media, and accounts neither for changes in microstructure near the interface, nor for interfacial layers. High-resolution transmission electron micrographs of interfaces of deposited (Schroder, 1987) and SIMOX (Celler and White, 1992) amorphous silicon dioxide layers with silicon show no evidence of incomplete contact on length scales down to a few angstroms, nor of a different microstructure in the silicon near the boundary. These micrographs show only that the microstructures of the layers were not periodic up to the interface with the silicon. Two of the hypotheses discussed in Section 1, (*b*) a thickness-dependent microstructure or stoichiometry, and (*c*) thermal boundary resistances or interfacial layers, are not excluded.

When the diffuse mismatch model is employed at both boundaries, one-dimensional phonon conduction normal to a layer is analogous to radiation between diffuse gray walls in an absorbing medium. This problem has been solved for grey media, i.e., when the photon mean free path is independent of the photon frequency (e.g., Siegel and Howell, 1981). To estimate the energy transport for nongrey media, the solution for grey media can be integrated over all frequencies to yield Eqs. (2)–(4) with (Chen and Tien, 1993)

$$B=\frac{3}{4\left(\frac{1}{\alpha_0}+\frac{1}{\alpha_1}-1\right)} \tag{5}$$

This approximation assumes that phonon modes of different frequencies are independent, i.e., that they do not exchange energy. This approach provides a good estimate of *energy* transport in nongrey media, and is the best available.

3 Bulk Phonon Mean Free Path

Walton (1974), Matsumoto et al. (1977), and Love and Anderson (1990) each used three regimes for the frequency dependence of $\Lambda_{\omega,\text{bulk}}$ in amorphous silicon dioxide. The pre-

Nomenclature (cont.)

x_ω = dimensionless phonon frequency $=h_P\omega/(k_BT)$
y = dimension normal to substrate, m
$\alpha_{0,1}$ = phonon transmission coefficients from layer
Γ = gamma function
θ = Debye temperature, K
Λ_G = phonon mean free path limited by geometric scattering, m
Λ_s = phonon mean free path, m
$\Lambda_{s,b}$ = Bd = phonon mean free path limited by boundary scattering, m
Λ_ω = frequency-dependent phonon mean free path, m
$\Lambda_{\omega,\text{bulk}}$ = bulk frequency-dependent phonon mean free path, m
$\Lambda_{\omega,D}$ = frequency-dependent phonon mean free path limited by Rayleigh scattering, m
$\Lambda_{\omega,SR}$ = frequency-dependent phonon mean free path limited by scattering on structural relaxation, m
Λ_0 = frequency-independent phonon mean free path of Kittel (1949), m
λ_i = parameter, Eqs. (12) and (13), m^{-1}
λ_s = $2\pi v_s/\omega$ = phonon wavelength, m
ρ = mass density, kgm^{-3}
$\delta\rho$ = deviation in mass density, kgm^{-3}
ρ_e = electrical resistivity, Ωm
τ_0 = fitting parameter for Λ_{SR}, s
ω = phonon angular frequency, rads^{-1}
ω^* = $\omega\tau_0$ = dimensionless phonon frequency
ω_D = Debye angular frequency, rads^{-1}

Subscripts

A = property or parameter of bridge A
C = property or parameter of bridge C
D = property or parameter of bridge D

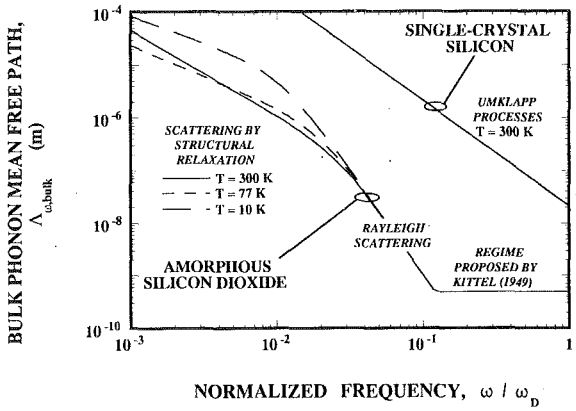

Fig. 3 The phonon mean free path in bulk amorphous silicon dioxide, $\Lambda_{\omega,bulk}$, showing the three regimes of its frequency dependence. Also shown is the mean free path in crystalline silicon limited by Umklapp scattering (Holland, 1963).

sent work uses the frequency dependence shown in Fig. 3, which combines expressions that are successful in each regime. For the *high-frequency regime*, $\omega > \sim 0.1\ \omega_D$, the frequency-independent phonon mean free path of Kittel (1949, 1986) is used, Λ_0. It is Λ_s in Eq. (1), calculated using thermal-conductivity and specific-heat data above 300 K (Sugawara, 1969; Touloukian and Buyco, 1970) where Λ_s varies little with temperature and phonons in the high-frequency regime dominate conduction. The average value between 300 and 500 K is used, $\Lambda_0 = 4.94$ Å.

In the *intermediate frequency regime*, $0.01\ \omega_D < \omega < 0.1\ \omega_D$, the mechanism responsible for phonon scattering is unknown. Freeman and Anderson (1986a) closely fitted the temperature dependence of the thermal conductivity of many amorphous solids, including silicon dioxide, using Eq. (2) and

$$\Lambda_{\omega,D} = \frac{S_D}{\omega^4}, \quad S_D = 1.76 \times 10^{42}\ \text{m rad}^4\text{s}^{-4} \tag{6}$$

This frequency dependence is analogous to the Rayleigh scattering of phonons on regions with different elastic properties and dimensions small compared to the wavelength (Ziman, 1960). For a region with a deviation in mass density $\delta\rho$ compared to the surrounding medium of density ρ, the phonon mean free path is given approximately by Eq. (6) and

$$S_D = \frac{144 v_s^4}{\pi N_D a^6} \left(\frac{\delta\rho}{\rho}\right)^{-2} \tag{7}$$

where N_D is the number density and a the typical dimension of the scattering sites. The opposing limit to Rayleigh scattering is geometric scattering for high-frequency phonons, which yields the frequency-independent mean free path $\Lambda_G = (N_D \pi a^2/4)^{-1}$. If this expression and Eq. (7) are solved for a and N_D using $\Lambda_G = \Lambda_0$ and $\delta\rho = \rho$, the volume of scattering sites exceeds the material volume. This indicates that if Rayleigh scattering occurs, Λ_0 is smaller than the corresponding geometrical-scattering limit.

The mean free paths of phonons in the *low-frequency regime*, $\omega < 0.01\ \omega_D$, are limited by *structural relaxation* and can be measured through the attenuation of sound waves (Hunklinger and Arnold, 1976). Structural relaxation is the rearrangement of atoms in the amorphous material due to elastic waves. The structural relaxation can occur out of phase with the long-wavelength phonons and absorb their energy. The theory for this phenomenon is similar to the Debye relaxation model, which determines the influence of electric dipoles in liquids on the photon mean free path (Bohren and Huffman, 1983). Gilroy and Phillips (1981) developed the *asymmetric double-well potential model* to describe phonon absorption by structural relaxation. Bonnet (1991) approximated their integrals, yielding

$$\frac{1}{\Lambda_{\omega,SR}} = \frac{\pi S_{SR} \omega}{2 v_s} \left[\sqrt{\pi}\, \frac{\Gamma\left(\frac{T^*}{2}+1\right)}{\Gamma\left(\frac{T^*}{2}+\frac{3}{2}\right)} \frac{T^*}{\cos\left(\frac{\pi}{2} T^*\right)} (\omega^*)^{T^*} - \frac{T^*}{1-T^*}\, \omega^* \right] \tag{8}$$

where $\Lambda_{\omega,SR}$ is the phonon mean free path limited by structural relaxation, $\omega^* = \omega\tau_0$, $T^* = k_B T/E_0$, and Γ is the gamma function. Bonnet (1991) closely fitted the data of Vacher et al. (1981) for amorphous silicon dioxide from 10 to 300 K using $\tau_0 = 2.5 \times 10^{-13}$, $E_0 = 5.02 \times 10^{-21}$ J, and $S_{SR} = 1.89 \times 10^{-3}$. These values and Eq. (8) are used here. Equation (6) models Rayleigh scattering in the intermediate frequency regime. The transition between the low and intermediate frequency regimes is modeled using Matthiessen's rule,

$$\frac{1}{\Lambda_{\omega,\text{bulk}}} = \frac{1}{\Lambda_{\omega,D}} + \frac{1}{\Lambda_{\omega,SR}} \tag{9}$$

The mean free path $\Lambda_{\omega,\text{bulk}}$ used here agrees well with the data of Vacher et al. (1981) at 3.5×10^{10} Hz and with the data of Jones et al. (1964) near 5×10^8 Hz at temperatures between 10 and 300 K. The mean free path also agrees with data presented by Love and Anderson (1990) near 3×10^{10} and 2×10^{11} Hz at 90 and 300 K. The only significant disagreement occurs at 2×10^{11} Hz at 90 K, where one measurement indicates a smaller mean free path than that shown in Fig. 3. But the value of $\Lambda_{\omega,\text{bulk}}$ at this frequency in Fig. 3 was obtained by fitting Eq. (2) to low-temperature thermal conductivity data, which are also relevant to the present work. The mean free path used here is very similar to that of Love and Anderson (1990). These authors used a slightly different model for scattering on structural relaxation than that developed by Gilroy and Phillips (1981), called the *symmetric double-well potential model*. It is not known which model is most appropriate for amorphous materials.

Figure 3 shows the phonon mean free path in silicon at room temperature limited by Umklapp scattering (Holland, 1963). The room-temperature thermal conductivity of silicon is about two orders of magnitude larger than that of silicon dioxide, which is due almost entirely to the much larger mean free path of phonons. In silicon dioxide, phonons experiencing Rayleigh scattering are responsible for more of the specific heat at 77 K than at 300 K. Since these phonons have longer mean free paths than the high-frequency phonons, boundary scattering is more important at 77 K than at room temperature.

The effective conductivity of silicon dioxide layers is calculated using Eqs. (2)–(6), (8), and (9). From 10 to 300 K, the conductivity predicted using $d = \infty$ differs by up to 20 percent from bulk data. This is due to the approximate Debye model for the phonon density of states. In this work, the Debye model is assumed only to predict the *relative contributions* of phonons of different frequencies to the total conductivity. This allows the calculated $k_{n,\text{eff}}$ to be normalized by the k_{bulk} calculated using $d = \infty$. The final prediction for $k_{n,\text{eff}}$ is

$$k_{n,\text{eff}} = [k_{\text{bulk}}]_{\text{measured}} \times \left[\frac{k_{n,\text{eff}}}{k_{\text{bulk}}}\right]_{\text{calculated}} \tag{10}$$

4 Experimental Technique

4.1 Apparatus. Figure 4 is a cross section of the test structure. It is based on that used by Swartz and Pohl (1987) for thermal boundary resistance measurements. The width of bridge A is $w = 5$ μm, yielding nearly one-dimensional conduction normal to the sample layer. The width of the nonheating bridges is near 1 μm. Section 4.2 analyzes thermal

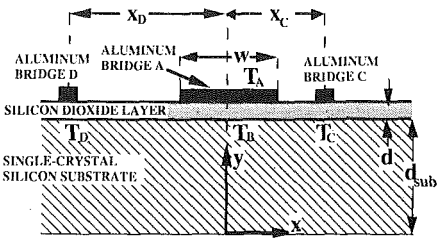

Fig. 4 Cross section of test structure used here to measure $k_{n,eff}$

conduction in the substrate, whose contribution to the uncertainty is estimated using a second nonheating bridge D. The center-to-center bridge separations are $x_C = 5.5$ μm and $x_D = 14.5$ μm. The temperature change that occurs when the heater bridge A is switched on, i.e., when it suddenly carries a large current, is ΔT. The temperature change ΔT_A is measured by bridge A, and ΔT_B is obtained from ΔT_C by modeling the heat conduction in the substrate. The conductivity $k_{n,\text{eff}}$ is calculated from the heater power Q and length L using

$$R_T = \frac{d}{k_{n,\text{eff}}} = \frac{\Delta T_A - \Delta T_B}{Q/(wL)} \tag{11}$$

The wafer is secured to a Temptronic Model TP38B temperature-control chuck, a copper disk with 88.9 mm diameter and thickness 19.1 mm, by means of suction through holes on the surface of the chuck. A thermocouple with one junction soldered to the chuck surface measures the test-structure temperature. The error due to this arrangement is determined using a second thermocouple attached to a wafer. The calibration of each bridge consists of determining the temperature derivative of its electrical resistance, which is affected by an error in the measured temperature *change* of the test structure. The relative uncertainty in the resistance thermometer calibration is found to be $U(\partial R_i/\partial T_i) = 0.04$ for all temperature changes between 273 and 423 K, where $U(q)$ is the relative uncertainty in the parameter q.

The bridge cross section is isothermal due to the low values of the thermal resistances for conduction normal to the bridge and across its cross section compared to the thermal resistance of the silicon dioxide layer. As a result, w in Eq. (11) is the width of the aluminum–silicon dioxide contact. Scanning electron microscopy yields the relative dimensions of the cross section of the bridge, from which w is calculated using the measured electrical resistivity of the bridge material and the length and electrical resistance of the bridge.

4.2 Substrate Thermal Conduction Analysis. The temperature change ΔT_B is calculated from the measured ΔT_C by solving the heat diffusion equation, $\nabla^2 T = 0$, in the substrate. Except for the thinnest layers, the difference between ΔT_B and ΔT_C is much less than ΔT_A, and approximations in this analysis have a small effect on the measurement. The model uses the two-dimensional coordinate system in Fig. 4 and the following approximations:

1 The effect of bridges C and D on conduction in the substrate is neglected. This results in a plane of symmetry and an adiabatic boundary condition at $x = 0$.

2 Substrate conduction is assumed to be two dimensional in the x–y plane. The ratio of the bridge length to the substrate thickness is approximately 4.2.

3 The wafer is assumed to possess a uniform temperature T_0 at $y = 0$.

4 The energy flux from bridge A, of width near 5 μm, is uniform in x and travels directly through the silicon dioxide layer, resulting in a heat-flux boundary condition at $y = d_{\text{sub}}$ of $-Q/(wL)$ for $0 < x < w/2$. This neglects the influence of spreading in the silicon dioxide on ΔT_B, but is estimated to yield a relative error of less than 1 percent in $k_{n,\text{eff}}$.

5 Conduction out of the substrate through the silicon dioxide to the air on top is neglected, yielding an adiabatic boundary condition at $y = d_{\text{sub}}$ for $x > w/2$.

6 The substrate side boundaries are assumed to be far from the heater compared to d_{sub}. The boundary condition there has no effect on the temperature near the heater. The boundary condition $T = T_0$ at $x = W$ and the requirement $W/d_{\text{sub}} \gg 1$ are used.

Separation of variables yields ΔT_C and ΔT_D,

$$\Delta T_{C,D} = \frac{2Q}{LwWk_{\text{sub}}} \sum_{i=0}^{\infty} \tanh(\lambda_i d_{\text{sub}}) \frac{\sin(\lambda_i w/2)\cos(\lambda_i x_{C,D})}{(\lambda_i)^2},$$

$$\lambda_i = \frac{\pi}{W}\left(\frac{2i+1}{2}\right), \quad W \gg d_{\text{sub}} \tag{12}$$

The average temperature at the interface of the silicon and the silicon-dioxide underneath the heater bridge is the average value of Eq. (12) for $0 < x < w/2$,

$$\Delta T_B = \frac{4Q}{Lw^2Wk} \sum_{i=0}^{\infty} \tanh(\lambda_i d_{\text{sub}}) \frac{\sin^2(\lambda_i w/2)}{(\lambda_i)^3} \tag{13}$$

The temperature difference ΔT_B for Eq. (11) is

$$[\Delta T_B]_{\text{experiment}} = [\Delta T_C]_{\text{experiment}} + [\Delta T_B - \Delta T_C]_{\text{analysis}} \tag{14}$$

The normalized uncertainty due to the approximate thermal-conduction analysis is estimated from the difference between the predicted and measured temperatures of bridges C and D,

$$U([\Delta T_B - \Delta T_C]_{\text{analysis}}) = \frac{[\Delta T_C - \Delta T_D]_{\text{experiment}} - [\Delta T_C - \Delta T_D]_{\text{analysis}}}{[\Delta T_C - \Delta T_D]_{\text{experiment}}} \tag{15}$$

4.3 Uncertainty Analysis. The thermal resistance determined in these experiments is related to the measured quantities by

$$R_T = \frac{[\Delta T_A]_{\text{experiment}} - [\Delta T_C]_{\text{experiment}} - [\Delta T_B - \Delta T_C]_{\text{analysis}}}{Q/(wL)}$$

$$= \frac{\left[\Delta\left(\frac{V_A}{I_A}\right)\left(\frac{dR_A}{dT_A}\right)^{-1} - \frac{\Delta V_C}{I_C}\left(\frac{dR_C}{dT_C}\right)^{-1} - [\Delta T_B - \Delta T_C]_{\text{analysis}}\right]}{I_A V_A/(wL)} \tag{16}$$

where V_A, I_A, V_C, and I_C are the voltage drops and currents measured for bridges A and C. The quantities $\Delta(V_A/I_A)$ and $\Delta(V_C/I_C)$ are the changes of the resistances of bridges A and C, which occur when the heater bridge turns on. The current I_C is very stable, but I_A, V_A, and V_C experience small fluctuations in time, which are used for their uncertainties here. The uncertainty in the bridge length L is negligible. For simplicity, the uncertainties in $\Delta(V_A/I_A)$ and ΔV_A are treated as independent. The total uncertainty in the thermal resistance is calculated using Eq. (16) and the sum-of-squares technique (Holman, 1984),

$$[U(R_T)]^2 = \left[U\left(\frac{dR_A}{dT_A}\right)\right]^2\left[\frac{\Delta T_A}{\Delta T_A - \Delta T_B}\right]^2 + \left[U\left(\Delta\left(\frac{V_A}{I_A}\right)\right)\right]^2\left[\frac{\Delta T_A}{\Delta T_A - \Delta T_B}\right]^2 + \left[U\left(\frac{dR_C}{dT_C}\right)\right]^2\left[\frac{\Delta T_C}{\Delta T_A - \Delta T_B}\right]^2 + [U(\Delta V_C)]^2\left[\frac{\Delta T_C}{\Delta T_A - \Delta T_B}\right]^2 + [U([\Delta T_B - \Delta T_C]_{\text{analysis}})]^2\left[\frac{\Delta T_B - \Delta T_C}{\Delta T_A - \Delta T_B}\right]^2 + [U(V_A)]^2 + [U(I_A)]^2 + [U(w)]^2 \tag{17}$$

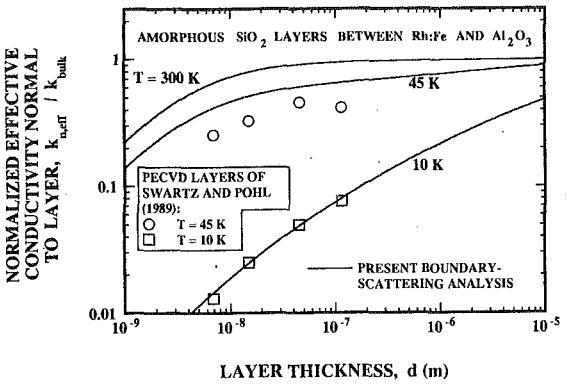

Fig. 5 Predictions of the thermal conductivity ratio $k_{n,eff}/k_{bulk}$ considering phonon-boundary scattering, compared with data for PECVD silicon-dioxide layers

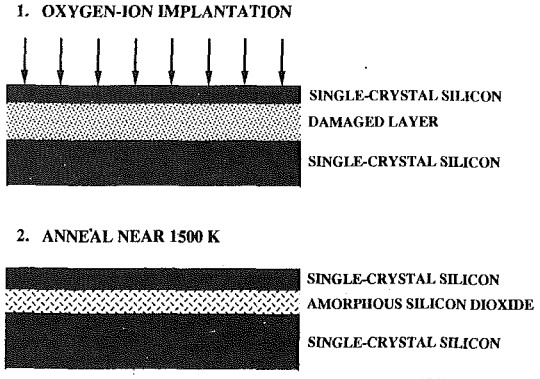

Fig. 6 Separation by implantation with oxygen (SIMOX) fabrication process (e.g., Celler and White, 1992)

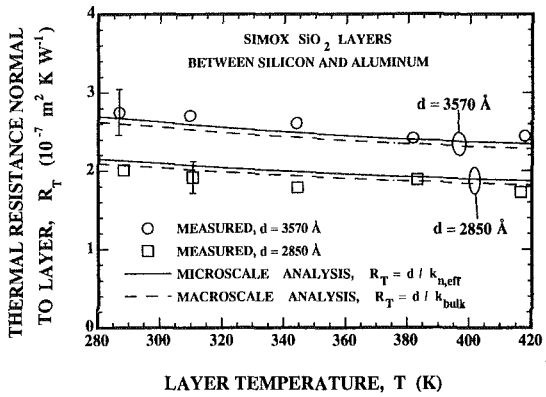

Fig. 7 Comparison of boundary-scattering (microscale) analysis with data for SIMOX silicon-dioxide layers

In the present work, this technique is applied to layers near 0.3 μm thick. For these layers, the approximate largest values of the terms on the right of Eq. (17) are $(0.056)^2$, $(0.034)^2$, $(0.032)^2$, $(0.032)^2$, $(0.028)^2$, $(0.01)^2$, $(0.01)^2$, and $(0.063)^2$, yielding $U(R_T) = 0.106$. The uncertainty is dominated by the uncertainties of the width of bridge A and the calibration of bridge A. For much thinner layers, where $\Delta T_B - \Delta T_C$ can be comparable to $\Delta T_A - \Delta T_B$, the uncertainty due to the thermal analysis is significant (Goodson et al., 1993a). The present experimental technique is similar to those of Schafft et al. (1989) and Brotzen et al. (1992), because it uses a thin-layer bridge to heat the sample layer. But both sets of authors determined ΔT_B using the measured temperature at the *bottom* of the substrate. This temperature difference is always much larger than $\Delta T_B - \Delta T_C$, so that the approximations in the thermal-conduction analysis are much more important than those used here. It is important to minimize this component of the uncertainty when measuring very thin layers, i.e., $d \leq 0.1$ μm. While this uncertainty was negligible in the measurements of Schafft et al. (1989) for layers thicker than 1 μm, its impact on the data of Brotzen et al. (1992) for layers as thin as 0.1 μm needs to be assessed.

5 Results and Discussion

Figure 5 compares the predictions of the phonon-boundary scattering analysis with the low-temperature data of Swartz and Pohl (1989) for PECVD silicon dioxide layers bounded by Rh:Fe, which is rhodium with a small fraction of iron, and sapphire. The data are represented in this plot using the k_{bulk} data of Zeller and Pohl (1971). Boundary scattering is more important at low temperatures where low-frequency phonons, which have long mean free paths, account for more of the conductivity. The agreement is excellent at 10 K for a range of thicknesses, which supports the use of Eqs. (2)–(5). This agreement relies heavily on the transmission coefficients calculated using the diffuse mismatch model of Swartz and Pohl (1989), because at this temperature many phonons travel ballistically between the boundaries without scattering internally. At 45 K, the ratio $k_{n,eff}/k_{bulk}$ is overpredicted by the present analysis. This would be consistent with the *agreement* at 10 K if the phonon mean free paths in the layers were the same as in Fig. 3 in the low and intermediate-frequency regimes, which are most important at low temperatures, but were less than those given in Fig. 3 in the high-frequency regime, which becomes important above about 10 K. But Fig. 3 may still be correct for bulk fused silicon dioxide, since this material may have a different microstructure than the PECVD layers. The poor agreement at 45 K may also be due to a failure of the diffuse mismatch model above 30 K. This failure was observed for many interfaces by Swartz and Pohl (1989), who argued that highly resistive interfacial layers at the interfaces could be responsible. Figure 5 shows that $k_{n,eff}/k_{bulk}$ is approximately unity at room temperature for layers thicker than a few hundred angstroms, i.e., phonon-boundary scattering is not important. This is also the case if the calculation is performed using the transmission coefficients from silicon dioxide into aluminum and silicon, which were the bounding materials for the layers whose conductivities are given in Fig. 1. But the data in Fig. 1 yield ratios $k_{n,eff}/k_{bulk}$ that are much smaller than unity, indicating that the problem at 45 K in Fig. 5 becomes more important at higher temperatures.

The data for the silicon dioxide layers fabricated using oxygen-ion implantation (SIMOX) are compared with the predictions of the boundary-scattering analysis. The test structures were made from SOI wafers provided by Ibis Corporation in Danvers, MA, using the SIMOX process, which is depicted in Fig. 6. Oxygen atoms are implanted into a lightly doped single-crystal silicon substrate, forming a damaged sublayer. After an anneal near 1500 K, a silicon-dioxide layer forms beneath a single-crystal silicon overlayer of thickness near 0.22 μm. Devices are usually fabricated from the silicon overlayer. In this work, the silicon overlayers are etched away and the test structures are deposited onto the exposed silicon-dioxide layers. Figure 7 compares the near-room-temperature data for the SIMOX layers with the predictions of the phonon-boundary scattering analysis. *Microscale* analysis considers phonon-boundary scattering, while *macroscale* analysis yields the volume resistance of a layer from the bulk conductivity. The microscale and macroscale predictions are within 3 percent of each other, i.e., boundary scattering is not important. The SIMOX data are consistent with the boundary-scattering analysis. But the 11 percent relative uncertainty of these data makes it impossible for them to confirm or refute the predictions.

The data show that the SIMOX fabrication technique results in layers that are far different than those fabricated using other techniques. The conductivities $k_{n,eff}$ of SIMOX layers agree

very well with k_{bulk}, which is a first for amorphous silicon dioxide layers and is in stark contrast to the data shown in Fig. 1. The dramatic difference between the conductivities reported here for SIMOX layers and those reported previously for deposited layers indicates that the microstructure of the SIMOX layers is different than those of the deposited layers. This may result from a difference in porosity between the deposited and the SIMOX layers. Deposition techniques can yield a porosity in layers, which can reduce their thermal conductivities (e.g., Lambropoulos et al., 1991), but it is unlikely that pores form in the SIMOX layers. Another possibility is that the high-temperature anneal of the SIMOX layers causes an atomic-scale reordering (e.g., Nagasima, 1972), which improves the conductivity. Goodson et al. (1993a) showed that annealing improved the thermal conductivity of LPCVD silicon dioxide layers by up to 23 percent.

The agreement of the SIMOX data with k_{bulk} provides evidence that both the microstructure and stoichiometry of the SIMOX layers closely resemble those in bulk samples. The absence of a thickness-dependent conductivity in these layers indicates that neither thermal boundary resistances nor highly resistive interfacial layers are present. These findings are important for the designers of SOI circuits, because they make it appropriate to use $k_{n,eff} = k_{bulk}$ rather than the much smaller values of $k_{n,eff}$ in Fig. 1. Based on the SIMOX data in Fig. 7, Goodson et al. (1993b) used $k_{n,eff} = k_{bulk}$ when modeling thermal conduction in the SIMOX silicon dioxide layers in SOI circuits. Since the temperature field in SOI circuits is very sensitive to the conductivity of the SIMOX layer, the close agreement of their predictions with their data for transistor channel temperatures is a confirmation of the thermal conductivity values reported here.

6 Conclusions and Recommendations

Phonon-boundary scattering is of little practical importance in silicon dioxide layers above room temperature. As a result, the low conductivities in Fig. 1 measured elsewhere must be attributed to a thickness-dependent microstructure or stoichiometry in the layers, to distinct, highly resistive interfacial layers, or to measurement uncertainties. The interfacial layer hypothesis is questionable. For an interfacial layer to contribute significantly to the total thermal resistance, it would need a thermal conductivity much smaller than the remainder of the amorphous silicon dioxide, which has a thermal conductivity among the lowest of any nonporous solid. A more plausible explanation is an increased porosity near the boundaries of the layer, which would also account for the thickness dependence of the effective thermal conductivity.

This work adapts the technique of Swartz and Pohl (1987) for room-temperature measurements of the thermal conductivity normal to layers with a relative uncertainty of ± 11 percent. The large or unknown uncertainties of existing techniques for this measurement show that there is a need for standardized techniques with well-known limitations, such as exist for bulk solids. The technique used here is recommended as a standard.

It is important to measure the conductivity of layers fabricated in the same way as those in the circuit for which the effective thermal conductivity is needed. An SOI circuit designer employing data from Fig. 1 rather than from Fig. 7 would overpredict the temperature of devices and interconnects, which might result in a circuit of lower performance because it was overdesigned for interconnect reliability.

Acknowledgments

The SOI wafers used in this study were provided by IBIS Corp. D. A. A. and L. T. S. acknowledge the support of the Semiconductor Research Corporation (SRC) under contracts 91-SP-080 and 92-SP-309. K. E. G. and L. T. S. were supported by academic fellowships from the Office of Naval Research and AT&T Bell Labs, respectively.

References

Berman, R., 1976, *Thermal Conduction in Solids*, Oxford University Press, Oxford, United Kingdom, Chap. 9, p. 23.

Bohren, C. F., and Huffman, D. R., 1983, *Absorption and Scattering of Light by Small Particles*, Wiley, New York, pp. 130–136, 259–265.

Bonnet, J. P., 1991, "On the Thermally Activated Structural Relaxation in Glasses," *J. Non-crystalline Solids*, Vol. 127, pp. 227–331.

Brotzen, F. R., Loos, P. J., and Brady, D. P., 1992, "Thermal Conductivity of Thin SiO_2 Films," *Thin Solid Films*, Vol. 207, pp. 197–201.

Callaway, J., 1959, "Model for Lattice Thermal Conductivity at Low Temperatures," *Phys. Rev.*, Vol. 113, pp. 1046–1051.

Celler, G. K., and White, A. E., 1992, "Buried Oxide and Silicide Formation by High-Dose Implantation in Silicon," *MRS Bulletin*, Vol. 17, June, pp. 40–46.

Chen, G., and Tien, C. L., 1993, "Thermal Conductivity of Quantum Well Structures," *J. Thermophysics and Heat Transfer*, Vol. 7, pp. 311–318.

Flik, M. I., and Tien, C. L., 1990, "Size Effect of the Thermal Conductivity of High-T_c Thin-Film Superconductors," ASME JOURNAL OF HEAT TRANSFER, Vol. 112, pp. 872–881.

Freeman, J. J., and Anderson, A. C., 1986a, "Normalized Thermal Conductivity of Amorphous Solids," in: *Phonon Scattering in Condensed Matter*, A. C. Anderson and J. P. Wolfe, eds., Vol. 5, pp. 32–34.

Freeman, J. J., and Anderson, A. C., 1986b, "Thermal Conductivity of Amorphous Solids," *Phys. Rev. B.*, Vol. 34, pp. 5684–5690.

Goodson, K. E., and Flik, M. I., 1992, "Effect of Microscale Thermal Conduction on the Packing Limit of Silicon-on-Insulator Electronic Devices," *IEEE Trans. Components, Hybrids, and Manufacturing Technology*, Vol. 15, pp. 715–722.

Goodson, K. E., Flik, M. I., Su, L. T., and Antoniadis, D. A., 1993a, "Annealing-Temperature Dependence of the Thermal Conductivity of LPCVD Silicon-Dioxide Layers," *IEEE Electron Device Letters*, Vol. 14, pp. 490–492.

Goodson, K. E., Flik, M. I., Su, L. T., and Antoniadis, D. A., 1993b, "Prediction and Measurement of Temperature Fields in Silicon-on-Insulator Electronic Circuits," *Solutions to CFD Benchmark Problems in Electronic Packaging*, ASME HTD-Vol. 255, D. Agonafer, ed., pp. 11–19; submitted to ASME JOURNAL OF HEAT TRANSFER.

Gilroy, K. S., and Phillips, W. A., 1981, "An Asymmetric Double-Well Potential Model for Structural Relaxation Processes in Amorphous Materials," *Philos. Mag.*, Vol. B42, pp. 735–746.

Guenther, A. H., and McIver, J. K., 1988, "The Role of Thermal Conductivity in the Pulsed Laser Damage Sensitivity of Optical Thin Films," *Thin Solid Films*, Vol. 163, pp. 203–214.

Holland, M. G., 1963, "Analysis of Lattice Thermal Conductivity," *Phys. Rev.*, Vol. 132, pp. 2461–2471.

Holman, J. P., 1984, *Experimental Methods for Engineers*, McGraw-Hill, New York, pp. 50–57.

Hunklinger, S., Arnold, W., 1976, "Ultrasonic Measurements in Amorphous Solids," in: *Physical Acoustics*, W. P. Mason and R. N. Thurston, eds., Vol. 12, pp. 155–209.

Jones, C. K., Klemens, P. G., and Rayne, J. A., 1964, "Temperature Dependence of Ultrasonic Attenuation in Fused Quartz up to 1 kMc/s," *Phys. Lett.*, Vol. 8, pp. 31–32.

Kittel, C., 1949, "Interpretation of the Thermal Conductivity of Glasses," *Phys. Rev.*, Vol. 75, pp. 972–974.

Kittel, C., 1986, *Introduction to Solid State Physics*, Wiley, New York, Chap. 17.

Kumar, S., and Vradis, G. C., 1991, "Thermal Conduction by Electrons Along Thin Films: Effects of Thickness According to Boltzmann Transport Theory," in: *Micromechanical Sensors, Actuators, and Systems*, D. Cho et al., eds., ASME DSC-Vol. 32, pp. 89–101.

Lambropoulos, J. C., Jolly, M. R., Amsden, C. A., Gilman, S. E., Sinicropi, M. J., Diakomihalis, D., and Jacobs, S. D., 1989, "Thermal Conductivity of Dielectric Thin Films," *J. Appl. Phys.*, Vol. 66, pp. 4230–4242.

Lambropoulos, J. C., Jacobs, S. D., Burns, S. J., Shaw-Klein, L., and Hwang, S. S., 1991, "Thermal Conductivity of Thin Films: Measurement and Microstructural Effects," in: *Thin Film Heat Transfer—Properties and Processing*, M. K. Alam et al., eds., ASME HTD-Vol. 184, pp. 21–32.

Little, W. A., 1959, "The Transport of Heat Between Dissimilar Solids at Low Temperatures," *Can. J. Phys.*, Vol. 37, pp. 334–349.

Love, M. S., and Anderson, A. C., 1990, "Estimate of Phonon Thermal Transport in Amorphous Materials Above 50 K," *Phys. Rev. B*, Vol. 42, pp. 1845–1847.

Matsumoto, D. S., Reynolds, C. L., and Anderson, A. C., 1977, "Thermal Boundary Resistance at Metal–Epoxy Interfaces," *Phys. Rev. B*, Vol. 16, pp. 3303–3307.

Nagasima, N., 1972, "Structure Analysis of Silicon Dioxide Films Formed by Oxidation of Silane," *J. Appl. Phys.*, Vol. 43, pp. 3378–3386.

Savvides, N., and Goldsmid, H. J., 1972, "Boundary Scattering of Phonons in Silicon Crystals at Room Temperature," *Phys. Lett.*, Vol. A41, pp. 193–194.

Schafft, H. A., Suehle, J. S., and Mirel, P. G. A., 1989, "Thermal Conductivity Measurements of Thin-Film Silicon Dioxide," *Proc. IEEE Int. Conf. on Microelectronic Test Structures*, Vol. 2, pp. 121–124.

Schroder, D. K., 1987, *Advanced MOS Devices*, Addison-Wesley, Reading, MA, pp. 204–206.

Siegel, R., and Howell, J. R., 1981, *Thermal Radiation Heat Transfer*, Hemisphere, New York, pp. 476–481.

Stephens, R. B., 1973, "Low-Temperature Specific Heat and Thermal Conductivity of Noncrystalline Solids," *Phys. Rev. B*, Vol. 8, pp. 2896–2905.

Sugawara, A., 1969, "Precise Determination of Thermal Conductivity of High Purity Fused Quartz from 0° to 650°C," *Physica*, Vol. 41, pp. 515–520.

Swartz, E. T., and Pohl, R. O., 1987, "Thermal Resistance at Interfaces," *Appl. Phys. Lett.*, Vol. 51, pp. 2200–2202.

Swartz, E. T., and Pohl, R. O., 1989, "Thermal Boundary Resistance," *Rev. Mod. Phys.*, Vol. 61, pp. 605–668.

Tien, C. L., Armaly, B. F., and Jagannathan, P. S., 1969, "Thermal Conductivity of Thin Metallic Films and Wires at Cryogenic Temperatures," *Proc. Eighth Conference on Thermal Conductivity*, C. Y. Ho and R. E. Taylor, eds., Plenum Press, New York, pp. 13–19.

Touloukian, Y. S., and Buyco, E. H., 1970, "Specific Heat: Nonmetallic Solids," *Thermophysical Properties of Matter*, Vol. 5, IFI/Plenum, New York.

Vacher, R., Pelous, J., Plicque, F., and Zarembowitch, A., 1981, "Ultrasonic and Brillouin Scattering Study of the Elastic Properties of Vitreous Silica Between 10 and 300 K," *J. Non-crystalline Solids*, Vol. 45, pp. 397–410.

Walton, D., 1974, "Random-Network Model, Density Fluctuation, and Thermal Conductivity of Glasses," *Solid State Comm.*, Vol. 14, pp. 335–339.

Zachariasen, W. H., 1932, "The Atomic Arrangement in Glass," *J. American Chemical Society*, Vol. 54, pp. 3841–3851.

Zaitlin, M. P., and Anderson, A. C., 1975, "Phonon Thermal Transport in Noncrystalline Materials," *Phys. Rev. B*, Vol. 12, pp. 4475–4486.

Zaitlin, M. P., Scherr, L. M., and Anderson, A. C., 1975, "Boundary Scattering of Phonons in Noncrystalline Materials," *Phys. Rev. B*, Vol. 12, pp. 4487–4492.

Zeller, R. C., and Pohl, R. O., 1971, "Thermal Conductivity and Specific Heat of Noncrystalline Solids," *Phys. Rev. B*, Vol. 4, pp. 2029–2041.

Zhu, D. M., and Anderson, A. C., 1990, "Low-Temperature Thermal Conductivity of a Glassy Epoxy–Epoxy Composite," *J. Low Temp. Phys.*, Vol. 80, pp. 153–160.

Ziman, J. M., 1960, *Electrons and Phonons*, Oxford University Press, Oxford, United Kingdom, pp. 221–223, 357–370, and 456–460.